LBL-18216
c.2

Lawrence Berkeley Laboratory

UNIVERSITY OF CALIFORNIA

RECEIVED
LAWRENCE
BERKELEY LABORATORY

OCT 9 1984

LIBRARY AND
DOCUMENTS SECTION

Materials & Molecular Research Division

CALCULATION AND COMPUTER SIMULATION OF THE PARABOLOIDAL MIRROR ANALYZER (PMA)

G. Liu, J.J. Barton, C.C. Bahr,
and D.A. Shirley

August 1984

TWO-WEEK LOAN COPY

This is a Library Circulating Copy which may be borrowed for two weeks.

Prepared for the U.S. Department of Energy under Contract DE-AC03-76SF00098

LBL-18216
c.2

DISCLAIMER

This document was prepared as an account of work sponsored by the United States Government. While this document is believed to contain correct information, neither the United States Government nor any agency thereof, nor the Regents of the University of California, nor any of their employees, makes any warranty, express or implied, or assumes any legal responsibility for the accuracy, completeness, or usefulness of any information, apparatus, product, or process disclosed, or represents that its use would not infringe privately owned rights. Reference herein to any specific commercial product, process, or service by its trade name, trademark, manufacturer, or otherwise, does not necessarily constitute or imply its endorsement, recommendation, or favoring by the United States Government or any agency thereof, or the Regents of the University of California. The views and opinions of authors expressed herein do not necessarily state or reflect those of the United States Government or any agency thereof or the Regents of the University of California.

LBL-18216

Calculation and Computer Simulation of the Paraboloidal Mirror Analyzer (PMA)

G. Liu,* J. J. Barton, C. C. Bahr, and D. A. Shirley

Materials and Molecular Research Division
Lawrence Berkeley Laboratory
and
Department of Chemistry
University of California
Berkeley, California 94720

ABSTRACT

A semianalytical method is proposed to calculate the electric field and electron motion inside the paraboloidal electron mirror. The error of field calculation is not more than 0.01 percent and that of electron motion calculation is not more than 0.1 percent. Calculation and computer simulation show that such an electron mirror can give very good angle resolution even for electrons having a wide energy spectrum.

*Permanent Address: Department of Physics, Zhejiang University, Hangzhou, People's Republic of China.

INTRODUCTION

In many important studies of solid-state surfaces by means of photoelectron spectroscopy[1-12] a sensitive angle-resolving electron energy analyzer is required. The earliest designs for such analyzers placed a simple high-gain detector behind a conventional electrostatic analyzer with a small entrance aperture to select the energy and angle for the measurement.[13-15] Since only a tiny fraction of the total electron emission from the sample is collected by such an analyzer, only experiments with very high electron flux are feasible with this apparatus.

Two improvements to the collection efficiency of angle-resolved analyzers have been introduced. First, the output of an electrostatic analyzer has been fitted with a multichannel energy detector to increase the efficiency by an order of magnitude.[9] Specifically, a hemispherical analyzer presents a range of energies across the region between its inner and outer hemispheres: a position encoding detector then assigns energy based on position. Second, a large aperture band-pass analyzer has been equipped with a multichannel position encoder to read out angles.[16] Here an ellipsoidal electron mirror serves as a low-pass filter and the high-pass is provided by an electron retarding grid. The collection area, and hence the efficiency of this device, is three orders of magnitude larger than the simplest angle resolved analyzer.

Recently, a new analyzer for use with synchrotron radiation has been proposed[17] which is both multichannel in energy and

multichannel in angle. The concept is to direct the electrons from a point source to a position encoding detector with a paraboloidal electron mirror while measuring the electron time-of-flight to give the energy. The design of this analyzer, the time-and-position-encoding detector, and the computer control system will be described elsewhere. In this report we examine a tractable numerical model for the electrostatic paraboloidal electron mirror to ascertain to what extent it allows both angle and energy resolutions.

We shall show that an important compensation effect exists which brings electrons with different energies, but the same emission angle to the same position on the detector, thus achieving high angle resolution even for non-monochromatic electrons.

Fig 1. shows schematically the principle of the analyzer. The electron mirror M consists of a grid and a back plate, called the "reflector". Both of them have the same shape as a part of a paraboloid of revolution, and one is just a small displacement of the other along the symmetrical axis. The source point S is located on the axis of the paraboloid somewhere between the foci of the grid and the reflector. Ideally, electrons coming from S with different polar and azimuthal angles would be reflected by different portions on the mirror into parallel beams and then hit the detector D at different positions.

Practically, however, there are several factors causing the electron motion to depart from the ideal case, as follows:

(1) Reflected electron beams from different portions of the

mirror make different angles with the paraboloidal axis, which we call the exit angle deviations. This is caused by the electron motion within the finite field gap of the mirror and prevents electrons from hitting the correct position on the detector.

(2) Electrons with different energies incident at the same point on the mirror will exit at different points. This prevents these electrons from hitting the same position on the detector even if the exit beams are parallel to the paraboloidal axis.

(3) Effect of finite source size. This causes aberrations even when the mirror could be exactly the same as its ideal optical analogy.

With these problems in mind, and to make things clearer gradually, our discussion will have three parts:

(i) Electric field calculation of the paraboloidal mirror,

(ii) Calculation of electron motion within the field gap, and

(iii) Computer simulation of the angle resolution.

1. Calculation of Electric Field

Taking the cylindrical coordinates (R,ϕ,Z), with Z as the axis of the paraboloids and the focus of the grid as the origin, the equation of the grid surface can be expressed as (cf. Fig. 2)

$$Z_1 = \frac{p}{2} - \frac{R^2}{2p} \qquad (1)$$

and that of the reflector surface will be

$$Z_2 = H + \frac{p}{2} - \frac{R^2}{2p} \tag{2}$$

where the parameter p is twice the focal length of the paraboloids and H is the gap width (along Z direction). In our case p is 30.4 cm and H is 0.48 cm. Therefore, the electric field is confined within a very thin curved region.

The axial distance of a point P(R,Z) inside the gap to the grid surface is

$$Z - Z_1 = Z - \frac{p}{2} + \frac{R^2}{2p}$$

whose range is between 0 and H. Therefore, by making the transformation

$$r = \frac{R}{p} \tag{3}$$

$$u = \frac{Z-Z}{p} = \frac{Z}{p} - \frac{1-r^2}{2} \tag{4}$$

we transform the pair of mutually parallel paraboloids into a pair of parallel planes whose cross section is shown in Fig. 3. We shall show that the new coordinate system greatly simplifies the calculation.

In the new coordinate system (r,u) the field equations are

$$\frac{dE_z}{dr} + r\frac{dE_z}{du} - \frac{dE_R}{du} = 0 \qquad (\text{i.e. } \nabla \times E = 0) \tag{5}$$

$$\frac{dE_R}{dr} + r\frac{dE_R}{du} + \frac{dE_R}{dr} + \frac{dE_z}{du} = 0 \qquad \text{(i.e. } \nabla\cdot E = 0) \qquad (6)$$

$$\frac{d^2\phi}{dr^2} + (1+r^2)\frac{d^2\phi}{du^2} + 2r\frac{d^2\phi}{drdu} + \frac{1}{r}\frac{d\phi}{dr} + 2\frac{d\phi}{du} = 0 \qquad \text{(i.e. } \nabla^2\phi = 0) \qquad (7)$$

where $E = -\nabla\phi$ is the electrostatic field strength and ϕ the electrostatic potential. The boundary conditions for potential and field components are

$$\phi = 0 \qquad \text{at} \qquad u = 0 \qquad (8)$$

$$\phi = -V \qquad \text{at} \qquad u = h \qquad (9)$$

$$E_R = rE_z \qquad \text{at} \qquad u = 0,h \qquad (10)$$

where $-V$ is the negative voltage applied between the grid and the reflector and $h = H/p$. We notice that the slope on the grid or reflector surface is just

$$\tan\psi = \left|\frac{dZ}{dR}\right| = \frac{R}{p} = r$$

Therefore (10) is simply the vanishing of the tangential field component on the metallic boundaries.

Equations (5) ~ (7) seem at first glance a little complicated. Actually, as we shall see, it is not necessary to solve the second-order potential equation, and the equations for field components are easily solved by successive approximations.

We first notice that the value of u is always very small ($0 < u <$

h), so we can expand E_z and E_R into power series of u, i.e.

$$E_z = \frac{V}{H} \sum_n A_n u^n \tag{11}$$

$$E_R = \frac{V}{H} \sum_n B_n u^n \tag{12}$$

where A_n's and B_n's are functions of r only. We shall later see that all A_n's are of the same order of magnitude and so are all B_n's, so the expansions (11) and (12) converges rapidly.

Substituting (11) and (12) into (5) and (6), equating equal powers of u, we obtain the following recurrence relations for A_n's and B_n's:

$$rA_{n+1} - B_{n+1} = -\frac{1}{n+1}\frac{dA_n}{dr} \tag{13}$$

$$A_{n+1} + rB_{n+1} = -\frac{1}{n+1}\left(\frac{dB_n}{dr} + \frac{B_n}{r}\right) \tag{14}$$

After rearrangement they become

$$A_{n+1} = -\frac{1}{(n+1)(1+r^2)}\left[r\frac{dA_n}{dr} + \frac{dB_n}{dr} + \frac{B_n}{r}\right] \tag{15}$$

$$B_{n+1} = \frac{1}{(n+1)(1+r^2)}\left[\frac{dA_n}{dr} - r\frac{dB_n}{dr} - B_n\right] \tag{16}$$

where each of the A_n's and B_n's is determined by those of order n-1.

The potential at any point (r,u) can be obtained by integrating

E_z from the boundary point (r,0) to the field point (r,u)

$$\phi(r,u) = -p\int_0^u E_u \, du = -\frac{V}{h}\sum_n \frac{A_n}{n+1} u^{n+1} \tag{17}$$

and since $\phi(r,h/p) = -V$, it gives

$$\sum_n \frac{A_n}{n+1} h^n = 1 \tag{18}$$

This relation, together with (10) i.e.

$$B_0 = rA_0 \tag{19}$$

determines A_0 and B_0.

Now let us proceed to the first several approximations:

(1) ZEROTH-ORDER APPROXIMATION

In this approximation, the field is independent of u

$$E_Z^{(0)} = \frac{V}{H} A_0^{(0)} \tag{20}$$

$$E_R^{(0)} = \frac{V}{H} B_0^{(0)} \tag{21}$$

and (18) and (19) give

$$A_0^{(0)} = 1 \tag{22}$$

$$B_0^{(0)} = r \tag{23}$$

Therefore, E_Z is constant and E_R is proportional to r. The potential at any point is now given by

$$\phi = -p\int_0^u E_Z\, du = -\frac{V}{h}\, u \tag{24}$$

which is linear in u but independent of r. This implies the zeroth-order equipotential surfaces are a set of equally spaced paraboloids of the same shape as that of the grid and the reflector.

(2) 1st-ORDER APPROXIMATION

In this approximation the field components can be expressed as

$$E_Z^{(1)} = \frac{V}{H}\,(A_0^{(1)} + A_1^{(0)}u) \tag{25}$$

$$E_R^{(1)} = \frac{V}{H}\,(B_0^{(1)} + B_1^{(0)}u) \tag{26}$$

where $A_0^{(1)}$ and $B_0^{(1)}$ are 1st-order A_0 and B_0 respectively. We should note that the 1st-order A_1 and B_1 are now replaced by the Zeroth-order ones. Such a replacement simplifies the calculation greatly without losing much accuracy, since the error it would introduce is of the same order as that due to neglecting terms higher than u in (11) and (12). Now $A_1^{(0)}$ and $B_1^{(0)}$ can be determined from $A_0^{(0)}$ and $B_0^{(0)}$ by using the recursion formulae (15) and (16), giving

$$A_1^{(0)} = -\frac{2}{1+r^2} \tag{27}$$

$$B_1^{(0)} = -\frac{2r}{1+r^2} \tag{28}$$

while $A_0^{(1)}$ and $B_0^{(1)}$ are determined by (18) and (19), giving

$$A_0^{(1)} = 1 + \frac{h}{1+r^2} \tag{29}$$

$$B_0^{(1)} = r\ (1+ \frac{h}{1+r^2}) \tag{30}$$

Therefore, the 1st-order field components become finally

$$E_Z^{(1)} = \frac{V}{H}\ (1 + \frac{h}{1+r^2} - \frac{2u}{1+r^2}) \tag{31}$$

$$E_R^{(1)} = \frac{V}{H}\ r(1 + \frac{h}{1+r^2} - \frac{2u}{1+r^2}) \tag{32}$$

and the potential at a point (r,u) becomes

$$\begin{aligned} \phi^{(1)} &= - p\int_0^u E_u du = - \frac{pV}{H}\ [(1 + \frac{h}{1+r^2})u - \frac{u^2}{1+r^2}] \\ &= - \frac{V}{h}\ u\ [1+\frac{h-u}{1+r^2}] \end{aligned} \tag{33}$$

Since the term $(h-u)/(1+r^2)$ is much smaller than 1, the equipotentials deviate only slightly from parallel paraboloids.

(3) 2nd-order approximation

In this approximation the field components can be expressed as

$$E_Z^{(2)} = \frac{V}{H}\ (A_0^{(2)} + A_1^{(1)}u + A_2^{(0)}u^2) \tag{34}$$

$$E_R^{(2)} = \frac{V}{H}\ (B_0^{(2)} + B_1^{(1)}u + B_2^{(0)}u^2) \tag{35}$$

where $A_0^{(2)}$ and $B_0^{(2)}$ are 2nd-order A_0 and B_0, $A_1^{(1)}$

and $B_1^{(1)}$ are 1st-order A_1 and B_1, while $A_2^{(0)}$ and $B_2^{(0)}$ are zeroth-order A_2 and B_2. Our reasoning is the same as before. By using (15), (16), (18), and (19), we obtain

$$A_2^{(0)} = \frac{2(1+r^2)}{(1+r^2)^3} \tag{36}$$

$$B_2^{(0)} = \frac{4r}{(1+r^2)^3} \tag{37}$$

$$A_1^{(1)} = -\frac{2}{1+r^2}\left[1 - \frac{1-r^2}{(1+r^2)^2}h\right] = -\frac{2}{1+r^2} + \frac{2(1-r^2)}{(1+r^2)^3}h \tag{38}$$

$$B_1^{(1)} = -\frac{2r}{1+r^2}\left[1 + \frac{2}{(1+r^2)^2}h\right] = -\frac{2r}{1+r^2} - \frac{4r}{(1+r^2)^3}h \tag{39}$$

$$A_0^{(2)} = 1 + \frac{1}{1+r^2}h + \frac{1-r^2}{3(1+r^2)^3}h^2 \tag{40}$$

$$B_0^{(2)} = r + \frac{r}{1+r^2}h + \frac{r(1-r^2)}{3(1+r^2)^3}h^2 \tag{41}$$

Therefore the final expressions for the 2nd-order field components and potential shall be

$$E_Z^{(2)} = \frac{V}{H}\left\{1 + \frac{h-2u}{1+r^2} + \frac{1-r^2}{3(1+r^2)^3}\left[h^2 - 6hu + 6u^2\right]\right\} \tag{42}$$

$$E_R^{(2)} = \frac{V}{H}r\left\{1 + \frac{h-2u}{1+r^2} + \frac{1}{3(1+r^2)^3}\left[(1-r^2)h^2 - 12hu - 12u^2\right]\right\} \tag{43}$$

$$\phi^{(2)} = -\frac{V}{H}u\left\{1 + \frac{h-u}{1+r^2} - \frac{1-r^2}{3(1+r^2)^3}\left[h^2 - 3hu + 2u^2\right]\right\} \tag{44}$$

We notice that the equipotentials still differ only slightly from that in the zero-order approximation.

Figure 4 shows an equipotential plot obtained from 2nd-order calculation, but actually you cannot tell the difference between zeroth, 1st and 2nd calculations from such a plot.

Now let us make some quantitative estimation of the accuracy of different orders of approximation. First, the relative difference between 1st- and zeroth-values can be considered as the error of the zeroth-order calculation. For example, the error of E_Z will approximately be

$$\frac{\Delta E_Z}{E_Z} = \left| \frac{E_Z^{(1)} - E_Z^{(0)}}{E_Z^{(1)}} \right| = \frac{h}{1+r^2} \tag{45}$$

In our practical case, h = 0.0158, the smallest value of r is 0.132, giving the maximum of $\Delta E_Z/E_Z = 0.0155$ which is not more than 2 percent. For E_R and ϕ we all have the same relative error.

Second, the relative difference beween 2nd- and 1st-values can be considered as the relative error of the 1st-order calculation. Therefore the relative error of E_Z in the first-order calculation will be

$$\frac{\Delta E_Z}{E_Z} = \left| \frac{E_Z^{(2)} - E_Z^{(1)}}{E_Z^{(2)}} \right| = \frac{1-r^2}{3(1+r^2)^3} [h^2 - 6hu + 6u^2] \tag{46}$$

which has a greatest value for u = 0 and u = h:

$$\frac{\Delta E_Z}{E_Z} = \frac{1-r^2}{3(1+r^2)^3} h^2 \tag{47}$$

By substituting the values $h = 0.0158$, $r = 0.132$ we obtain $\Delta E_Z/E_Z = 0.0000776$ which is smaller than 0.01 percent. For E_R and ϕ, we have same results of error estimation.

The above error estimation shows that the accuracy of 1st-order calculation is enough in many practical cases. So our analysis of electron motion will be based on this order of field calculation.

2. Analysis of Electron Motion

Before we proceed to analyze the electron motion we should note that

(1) Since the electron mirror has a finite size, the above field calculation is valid only at points which are not near the mirror edge. Our following calculation of electron motion inside the field gap of the mirror is valid also only at such points.

(2) With the preceding assumption, the electric field inside the mirror gap is cylindrically symmetrical. However, the electron motion is generally not cylindrically symmetrical, unless the source point is exactly on the axis of the paraboloid.

(3) The coordinate u we used above is not an inertial frame of reference. We should transform back to an inertial

coordinate, say

$$z = \frac{Z}{p} = u + \frac{1-r^2}{2} \tag{48}$$

before writing down the equations of motion.

Now, by using the 1st-order solution of the electric field, the 3-dimensional equations of motion can be written as

$$\ddot{z} = -c(1 + \frac{h-2u}{1+r^2}) = - c - c \frac{h-2u}{1+r^2} \tag{49}$$

$$\ddot{x} = - cx(1 + \frac{h-2u}{1+r^2}) = - cx - cx \frac{h-2u}{1+r^2} \tag{50}$$

$$\ddot{y} = -cy(1 + \frac{h-2u}{1+r^2}) = - cy - cy \frac{h-2u}{1+r^2} \tag{51}$$

where z, x, y are dimensionless variables and $x = r \cos \phi$, $y = r \sin \phi$, where ϕ is the azimuthal angle. $c = eV/2pH$ is a constant determined by the geometry and the mirror voltage applied.

Let us first neglect the second term on the right hand side of (49), (50), and (51) and search for the zeroth-order solution, getting

$$z = z_1 + \dot{z}_0 t - \frac{1}{2} ct^2 \tag{52}$$

$$x = x_1 \cos qt + \frac{\dot{x}_0}{q} \sin qt \tag{53}$$

$$y = y_1 \cos qt + \frac{\dot{y}_0}{q} \sin qt \tag{54}$$

where $q = \sqrt{c}$, z_1, x_1, y_1 are coordinates of the electron incident point on the mirror grid (satisfying the relation $z_1 = (1 - x_1^2 - y_1^2)/2$) and $\dot{z}_0$, $\dot{x}_0$, and $\dot{y}_0$ are "velocity" components of the incident electron. If z_0, x_0, y_0 are coordinates of the source point, E_x is the kinetic energy of the electron, we have

$$\dot{x}_0 = \sqrt{\frac{2E_k}{m}}\,\frac{x_1-x_0}{pd} = \sqrt{\frac{2E_k}{m}}\,\frac{x_1-x_0}{D} \tag{55}$$

$$\dot{y}_0 = \sqrt{\frac{2E_k}{m}}\,\frac{y_1-y_0}{pd} = \sqrt{\frac{2E_k}{m}}\,\frac{y_1-y_0}{D} \tag{56}$$

$$\dot{z}_0 = \sqrt{\frac{2E_k}{m}}\,\frac{z_1-z_0}{pd} = \sqrt{\frac{2E_k}{m}}\,\frac{z_1-z_0}{D} \tag{57}$$

where $D = p\sqrt{(x_1-x_0)^2+(y_1-y_0)^2+(z_1-z_0)^2}$ is the distance between source point and incident point on the mirror grid (see Fig. 5).

From (52) - (54) we can determine the variable u:

$$u = z - \frac{1}{2} + \frac{x^2+y^2}{2}$$

$$= \dot{z}_0 t - \frac{1}{2}ct^2 + \frac{x_1\dot{x}_0+y_1\dot{y}_0}{q}\sin qt\cos qt - \frac{1}{2}\left(x_1^2+y_1^2 - \frac{\dot{x}_0^2+\dot{y}_0^2}{C}\right)\sin^2 qt \tag{58}$$

$u = 0$ gives two solutions of t, one is the electron incident time $t = 0$. The other is the electron exit time $t = t_e$. Obviously t_e can only be determined numerically even in this zeroth-order

approximation. However, we can make a rough estimation of t_e by assuming $qt_e << 1$, getting

$$t_e = \frac{2(\dot{z}_0+x_1\dot{x}_0+y_1\dot{y}_0)}{c(1+x_1^2+y_1^2)-x_0^2-y_0^2} \tag{59}$$

This expression is useful later.

Now let us return to equations (49) - (51). We know in our practical case the correction due to the second term on the right hand side of them is not more than 1.55 percent, so we can neglect any variation of this term due to variation of x or y without introducing much error.[18] This means we replace (49) - (51) by

$$\ddot{z} = - c - c\frac{h-2u}{1+x_1^2+y_1^2} \tag{60}$$

$$\ddot{x} = -cx - cx_1\frac{h-2u}{1+x_1^2+y_1^2} \tag{61}$$

$$\ddot{y} = - cy - cy_1\frac{h-2u}{1+x_1^2+y_1^2} \tag{62}$$

Substituting the zeroth-order u of (58) in to the second term of (60) - (62), solving for 1st-order z, x, y, we get

$$z = z_1 - \frac{c_3}{4} + (\dot{z}_0-\frac{q}{2}c_4)t - \frac{c}{2}(1+c_0)t^2 - \frac{c}{6}qt^3 - \frac{c}{12}c_2t^4$$

$$+ \frac{1}{4}c_3\cos 2qt + \frac{1}{4}c_4\sin 2qt \tag{63}$$

$$x = a_0 + a_1 t + a_2 t^2 + a_3 \cos 2\,qt + a_4 \sin 2\,qt + a_5 \cos qt + a_6 \sin qt \tag{64}$$

$$y = b_0 + b_1 t + b_2 t^2 + b_3 \cos 2qt + b_4 \sin 2qt + b_5 \cos qt + b_6 \sin qt \tag{65}$$

where

$$c_0 = \frac{2h + x_1^2 + y_1^2 - (\dot{x}_0^2 + \dot{y}_0^2)/c}{2(1 + x_1^2 + y_1^2)} \tag{66}$$

$$c_1 = -\frac{2\dot{z}_0}{1+x_1^2+y_1^2} \tag{67}$$

$$c_2 = \frac{c}{1+x_1^2+y_1^2} \tag{68}$$

$$c_3 = \frac{\dot{x}_0^2+\dot{y}_0^2-c(x_1^2+y_1^2)}{2c(1+x_1^2+y_1^2)} \tag{69}$$

$$c_4 = -\frac{x_1\dot{x}_0+y_1\dot{y}_0}{q(1+x_1^2+y_1^2)} \tag{70}$$

$$a_0 = x_1\left[\frac{2}{1+x_1^2+y_1^2} - c_0\right] \tag{71}$$

$$a_1 = -x_1 c_1 \tag{72}$$

$$a_2 = -x_1 c_2 \tag{73}$$

$$a_3 = \frac{1}{3} x_1 c_3 \tag{74}$$

$$a_4 = \frac{1}{3} x_1 c_4 \tag{75}$$

$$a_5 = x_1 - a_0 - a_3 \tag{76}$$

$$a_6 = \frac{\dot{x}_0 - a_1}{q} - 2a_4 \tag{77}$$

$$b_0 = y_1 [\frac{2}{1+x_1^2+y_1^2} - c_0] \tag{78}$$

$$b_1 = - y_1 c_1 \tag{79}$$

$$b_2 = - y_1 c_2 \tag{80}$$

$$b_3 = \frac{1}{3} y_1 c_3 \tag{81}$$

$$b_4 = \frac{1}{3} y_1 c_4 \tag{82}$$

$$b_5 = y_1 - b_0 - b_3 \tag{83}$$

$$b_6 = \frac{\dot{y}_0 - b_1}{q} - 2b_4 \tag{84}$$

To determine the exit time t_e, we first construct the function

$$u(t) = z(t) - \frac{1}{2} [1-x(t)^2-y(t)^2] \tag{85}$$

and its derivative

$$\dot{u}(t) = \dot{z}(t) + x(t)\dot{x}(t) + y(t)\dot{y}(t) \tag{86}$$

then use Newton-Raphson iterative method to solve the equation

$$u(t) = 0 \tag{87}$$

numerically.

In Fig. 5 the curve $u(t) \sim t$ is shown schematically. We first choose an arbitrary value $t = t_0$ (usually the t_e value given by Eq. (59)) which we believe to be quite near the intersection point t_e on the t-axis. Then we draw a tangent to the curve at the point $y(t_0)$, which intersects the t-axis at $t = t_1$ given by

$$t_1 = t_0 - \frac{u(t_0)}{\dot{u}(t_0)} \tag{88}$$

Obviously t_1 is much nearer t_e than t_0 is. We can repeat the process by taking this t_1 as a new t_0 and finding the new t_1. The iterative process continues until the difference between t_0 and t_1 becomes smaller than a preset value, thus getting t_e.

The magnitude of t_e is important because it contributes up to several percent of the total flight time from the source to the detector. t_e also varies with incident angle, grid voltage and kinetic energy of the electrons. However, by careful examination of Eq. (63) ~ (65) we notice that if we consider the product qt as the reduced time, the dependence of all the coefficients on E_k and V will only be through the ratio E_k/W, where W is the energy

equivalence of the mirror voltage (i.e., $W = eV$). This means the product qt_e is uniquely determined by the ratio E_k/W, provided the geometry is given. We can also say that t_e is inverse proportional to V if E_k/W is fixed. This will facilitate the calculation since we can calculate t_e for one value of V and then extend the result to another V value by simply making a time scaling. Fig. 6 shows the product qt_e as a function of E_k/W for a definite geometry (p = 30.4 cm, H = 0.48 cm) and several incident directions. The numbers 1, 2, and 3 at the right hand side of the figure refer to the nearest (X_1 = 4 cm, Y_1 = 0), middle (X_1 = 7.5 cm, Y_1 = 0), and farthest (X_1 11 cm, Y_1 = 0) incident points, respectively. Together with the formula

$$q = 0.01098 \quad V \text{ (volts)} \quad \text{(cm/ns)} \tag{89}$$

t_e will be readily determined.

t_e is important not just by itself. From it we can calculate the position difference between the exit point and the incident point

$$\Delta X_1 = X(t_e) - X_1, \quad \Delta Y_1 = Y(t_e) - Y_1 \tag{90}$$

and the angle deviation of the exit beam from vertical downwards

$$\begin{aligned} \delta_x &= \arctan\,(-X(t_e)/Z(t_e)) \\ \delta_y &= \arctan\,(-Y(t_e)/Z(t_e)) \end{aligned} \tag{91}$$

The meaning of these quantities is obvious from Fig. 7, where the upper half is the side-view and the lower half is the top-view.

(x_0, y_0, z_0) represents the source point with the grid focus as the origin. The circle in the top view represents roughly the projection of the mirror on the horizontal plane.

Fig. 8 shows the position difference ΔX_1 as a function of E_k/W for three electron beams coming from the focus of the mirror grid with different emission angles. The numbers 1, 2 and 3 at the right hand side of the figure have the same meaning as in Fig. 6. The largest relative deivation appears at the nearest incident point and is equal to 0.238/4 = 0.0595. We also notice that the variation of ΔX_1 with E_k/W is almost linear.

Fig. 9 shows the exit-angle deviation δ_x as a function of E_k/W for the above mentioned three electron beams. The variation is also approximately linear. The negative values of δ_x means that the exit beams all tilt in towards the paraboloidal axis. Different δ_x values for different incident positions show that the exit beams are not parallel to each other.

Both the position differences ΔX_1, ΔY_1, and exit-angle deviations δ_x, δ_y contribute to the total position deviations on the detector face. If H_c is the distance between the vertex of the paraboloidal grid and the detector face, the distance between the electron exit point on the grid and the latter will be $H_c - p/2 + Z(t_e)$, and the total position deviations (from the projection of the incident point) on the detector face will be

$$\Delta X = \Delta X_1 + \delta_x(H_c - \frac{p}{2} + Z(t_e)) \qquad (92a)$$

$$\Delta Y = \Delta Y_1 + \delta_y(H_c - \frac{p}{2} + Z(t_e)) \qquad (92b)$$

However, the situation is now not worse but better, since the two terms at the right-hand-side of (92) can compensate each other, thus making ΔX and ΔY very small. For electrons with low energies ($E_k/W << 1$), both terms are negligible if the source point is at the focus of the grid, giving approximately zero position deviations on the detector face. This means that the low-energy electrons follow exactly a path determined by geometric optics with the paraboloidal grid as the optical mirror. For electrons with higher energies, we can achieve the compensation by proper adjustment of the geometrical parameters. This will be discussed in the next section.

3. Computer Simulation of Angle Resolution

(a) The Compensation Effect

Based on the preceding calculation and discussion, a computer program has been constructed to calculate the total position deviations on the detector face and to plot these deviations automatically. Since changing the electron energy has the same effect on the detector point as changing the emission angle, a equivalence relation between these two changes exists. Consider a low-energy ($E_k/W << 1$) electron beam emitted from the focus of the paraboloidal grid. The radial coordinate of the point where electrons are hitting the detector face is exactly that of the point where electrons are incident on the grid, i.e.

$$R = p \tan \frac{\theta}{2} . \tag{93}$$

Hence the equivalence relation between emission angle and position deviation is

$$\Delta R = \frac{p}{2} \sec^2 \frac{\theta}{2} \Delta\theta = \frac{p}{2} (1+R^2/p^2)\Delta\theta . \tag{94}$$

If we drop the small term R^2/p^2, the equivalence will be

$$\Delta R(\text{cm}) = \frac{\Delta\theta(\text{deg})}{3.77} \tag{95}$$

in our case ($p = 30.4$ cm).

Figs. 10 through 18 are drawn on the plane of the detector face to show the position deviations. The dotted curve, for which we assume a circular shape of radius R_c centered at a distance 7.5 cm away from the axis of the paraboloid, represents the projection of the points where electrons are entering the mirror. The broken curve represents the projection of the points where electrons are exiting the mirror. The solid curve represents points at which electrons are hitting the detector. The numbers labeled are values of the total position deviations in cm for several typical incident points.

Fig. 10 is obtained with the following parameters: $p = 30.4$ cm, $H = 0.48$ cm, $H_c = 39.8$ cm, $X_0 = Y_0 = Z_0 = 0$, $E_k/W = 1$ and $R_c = 3.5$ cm. The last number approximates the effective radius of the detector. We notice the compensation effect of the exit-angle deviation to the position deviation. The maximum absolute value

0.255 cm corresponds to 0.96° deviation of emission angle and is acceptable.

Fig. 11 is for low energy electrons ($E_k/W = 0.1$) under the same conditions. We can see that the position deviations are negligibly small. Therefore, for consideration of position accuracy, we can consider electrons with maximum energy ($E_k/W = 1$) only.

However, a plot of position deviation ΔX against incident position X_1 (lower curve of Fig. 19) shows that in the present case the maximum position deviation (absolute value) does not occur at the point $X_1 = 11$ cm but at the point $X_1 = 9$ cm. Therefore, it would be better to look at the circle with radius $R_c = 1.5$ cm instead of $R_c = 3.5$ cm. This is shown in Fig. 12. The maximum absolute value of position deviation is now 0.269 cm, which is equivalent to 1.01° deviation of emission angle, a little larger than that in the $R_c = 3.5$ cm case.

Figs. 13 through 17 show the effect of sample size by allowing the source point to move + or -1 mm along either one of the x, y, z axis. We can see that the maximum position deviation (absolute value) becomes now 0.469 cm, equivalent to a deviation of emission angle 1.77°.

(b) Optimal Compensation

We notice that the compensation shown in Fig. 10 is excessive. Actually, one can get an optimum compensation by a proper adjustment

of the distance H_c. Fig. 18 shows such a case, where H_c = 26.8 cm. (We note that in this figure, and from now on, the broken curve representing the projection of exit points is omitted for the sake of simplicity.) The maximum position deviation becomes now 0.029 cm, equivalent to a deviation of emission angle only 0.11° provided the source point is at the focus of the grid. Fig. 19 compares the position deviations for two cases at different incident positions along the x axis. If sample size effect is taken into account as we did before, calculation shows the maximum position deviation is 0.179, equivalent to an emission angle deviation 0.67°.

Sometimes a longer distance H_c is required by energy resolution and cannot be shortened arbitrarily. If this is the case and higher angle resolution is also preferred, one possible way to meet the goal is to replace the mirror by one with longer focal length.

(c) Effect of Retarding

In the actual construction of the analyzer, there is an additional grid midway between the mirror and detector (at a distance 27 cm from the detector face) on which a retarding potential V_R is applied, thus slowing down the electrons and improving the energy resolution. This potential is used for monoenergetic electrons or electrons with a narrow energy spectrum. However, this retarding potential has some effect to tilt the electron beam, thus increasing the position deviations on the detector face. Fig. 20 is an example

where the electron energy is $E_k/W = 0.9\sim1$ and the retarding voltage is $V_R/V = 0.8$. The meaning of the numbers labeled is the same as before. We can see that the largest position deviation is 1.177 cm, equivalent to a deviation in emission angle 4.44°. However, the situation can be improved by adjusting the source point. Fig. 21 shows that the position deviations are almost completely removed by shifting the source 0.4 cm upwards along the paraboloidal axis. Now the two solid circles coincide almost exactly with the dotted circle. Fig. 22 shows the best position z_0 for minimum position deviations at different retarding voltages in the present case ($E_k/W = 0.9\sim1$).

3. Discussion and Conclusions

The calculated results show that our semianalytical method for field and electron-motion calculation can be applied effectively to the paraboloidal electron mirror. This is a consequence of the extreme narrowness of the field gap that maintains the accuracy offered by series expansion and successive approximation. Ease of computation makes this approach desirable. If necessary, the coordinate-transformation step used in this method can also be combined with the finite-difference method to save mesh points.

The design concept of the paraboloidal mirror analyzer (PMA) was first stimulated by that of the ellipsoidal mirror analyzer (EMA).[16] However, like many others, the EMA is essentially an energy-resolved device. In the PMA case, the energy resolution is accomplished by the time-of-flight measurement and the position-sensitive detection performs a purely angle-resolved function. To ensure good angle resolution, a mechanism to get rid of energy dispersion is necessary. In the above "parallel grid-reflector" arrangement this goal is met by the compensation effect due to relatively large radial retarding field inside the gap. The radial distance between the grid and the reflector, as can be given by Equations (1) and (2), is

$$\Delta R = \frac{p}{R} H$$

which gives an approximate radial electric field (i.e., the zeroth-order field) proportional to R.

An alternative possibility is to choose a "confocal grid-reflector" arrangement, in which the focal length of the reflector is a little longer than that of the grid, but both foci coincide. In this case, Eq. (2) should be replaced by

$$Z_2 = H + \frac{p}{2} - \frac{R^2}{4H+2p}$$

and the radial distance ΔR becomes approximately

$$\Delta R = (\frac{R}{p} + \frac{p}{R})H$$

which gives a slightly weaker radial retarding field for the compensation, provided R/p is not too large. We also notice that the axial distance between grid and reflector is now approximately

$$Z_2 - Z_1 = (1 + \frac{R^2}{p^2})H$$

which increases slowly with increasing R, provided $R \ll p$.

In the actual construction of the paraboloidal electron mirror the grid and the reflector are held by several spherical beads between them. This makes the normal rather than axial distance between the grid and the reflector approximately a constant equal to the diameter of the beads. Now let us assume that this diameter equals H, the separation between grid and reflector at R = 0, then the axial distance between grid and reflector at any point becomes approximately

$$Z_2 - Z_1 = H \sec \frac{\theta}{2} = 1 + \frac{R^2}{p^2} H$$

and the radial distance also approximately equals

$$\Delta R = \frac{p^2+R^2}{R} H$$

Therefore, the actual case is by no means worse than the "confocal" case. The slightly weaker radial retarding field in comparison to the "parallel" case is even preferable for an optimum compensation at a longer mirror-detector distance H_c.

Acknowledgements

This work was supported by the Director, Office of Energy Research, Office of Basic Energy Sciences, Chemical Sciences Division of the U.S. Department of Energy under Contract No. DE-AC03-76SF00098.

References

1. D.A. Shirley, editor, Electron Spectroscopy (North-Holland, Amsterdam, 1972).

2. C.R. Brundle and A.D. Baker, editors, Electron Spectroscopy: Theory, Techniques and Applications (4 vols.) (Academic, New York, 1977-1981).

3. B. Feuerbacher, B. Fitton, and R.F. Willis, editors, Photoemission and Electronic Properties of Surfaces (Wiley, New York, 1978).

4. M. Cardona and L. Ley, editors, Photoemission in Solids (2 vols.) (Springer-Verlag, New York, 1978-79).

5. B. Feuerbacher and B. Fitton, in Electron Spectroscopy for Surface Analysis, edited by H. Ibach (Springer-Verlag, New York, 1977).

6. D.A. Shirley, J. Stohr, P.S. Wehner, R.S. Williams, and G. Apai, Phys. Scripta, 16, 398 (1977).

7. D.E. Eastman, in Vacuum Ultraviolet Radiation Physics, edited by E.E. Koch, R. Haensel, and C. Kunz (Pergamon, Vieweg, 1974).

8. L.F. Ley, J. Electron Spectrosc. Relat. Phenom. 15, 329 (1979).

9. S.D. Kevan, Lawrence Berkeley Laboratory Report LBL-11017, 1980.

10. R.F. Davis, Lawrence Berkeley Laboratory Report LBL-13511, 1981.

11. I. Lindau and W.E. Spicer, in Synchrotron Radiation Research, edited by H. Winick and S. Doniach (Plenum, New York, 1980).

12. D.A. Shirley, in Chemistry and Physics of Solid Surfaces (vol. III), edited by R. Vanselow and W. England (CRC, Boca Raton, 1982).

13. G.R. Apai, Lawrence Berkeley Laboratory Report, LBL-16906 (1977).

14. P.S. Wehner, Lawrence Berkeley Laboratory Report, LBL-7622 (1978).

15. R.S. Williams, Lawrence Berkeley Laboratory Report, LBL-7676 (1978).

16. D.E. Eastman, J.J. Donelton, N.C. Hien, and F.J. Himsel, Nuclear Instruments and Methods 172, 327 (1980).

17. J.J. Barton, S.W. Robey, C.C. Bahr, G. Liu, J. Katz, and D.A. Shirley, to be published.

18. Suppose the source is at or near the focus of the grid. The maximum position deviation of the exit point to the incident point on the mirror occurs at the nearest incident point X_1 = 4 cm, $Y_1 = 0$, giving $\Delta X = 0.238$ cm and $\Delta X/X_1 = 0.0595$. Hence the overall error due to replacement of X, Y by X_1, Y_1 in the second term of the right hand side of Eq. (50) is at most 0.0155 X 0.0595 = 0.000922, not more than 0.1 percent. Those of Eqs. (49) and (51) are even negligible.

Figure Captions

Fig. 1. Schematic representation of the paraboloidal mirror analyzer: S-electron source, M-mirror, D-detector.

Fig. 2. Mirror cross section in R-Z space: H-gap width along Z direction.

Fig. 3. Mirror cross section in r-u space: h-gap width in unit p.

Fig. 4. Equipotential plot of the paraboloidal electron mirror.

Fig. 5. Newton-Raphson method for solving the equation $u(t) = 0$.

Fig. 6. Dependence of flight-time inside field-gap on electron energy: $q = 0.01098$ V(volts) (cm/ns), W = eV.

Fig. 7. Diagram showing position deviation and exit-angle deviations on mirror grid: ΔX_1, ΔY_1-positions in cm, δ_x-angle deviation in XZ plane.

Fig. 8. Dependence of position difference between incident and exit points on electron energy: 1(X_1=4cm), 2(X_1=7.5cm), 3(X_1=11cm).

Fig. 9. Dependence of angle-deviation of exit beam on electron energy: 1(X_1=4cm), 2(X_1=7.5cm), 3(X_1=11cm).

Fig. 10. Diagram showing total position deviations on detector face: $H_c = 39.8$ cm, $R_c = 3.5$ cm, $X_0 = Y_0 = Z_0 = 0$. $E_k/W = 1$.

Fig. 11. Same as Fig. 10 except $E_k/W = 0.1$.

Fig. 12. Same as Fig. 10 except $R_c = 1.5$ cm.

Fig. 13. Same as Fig. 12 except $Z_0 = 0.1$ cm.

Fig. 14. Same as Fig. 12 except $Z_0 = -0.1$ cm.

Fig. 15. Same as Fig. 12 except $X_0 = 0.1$ cm.

Fig. 16. Same as Fig. 12 except $X_0 = -0.1$ cm.

Fig. 17. Same as Fig. 12 except $Y_0 = 0.1$ cm.

Fig. 18. Same as Fig. 12 except $H_c = 25.8$ cm.

Fig. 19. Dependence of position deviation on incident point.

Fig. 20. Diagram showing the effect of retarding potential on position deviations: $H_c = 39.8$ cm, $R_c = 1.5$ cm, $E_k/W = 1, 0.9$, $V_R/V = 0.8$, $X_0 = Y_0 = Z_0 = 0$.

Fig. 21. Same as Fig. 20 except $Z_0 = 0.4$ cm showing compensation of the effect of retarding potential by shifting the source point.

Fig. 22. Optimum source position under different retarding voltages ($H_c = 39.8$ cm, $E_k/W = 0.9 \sim 1$).

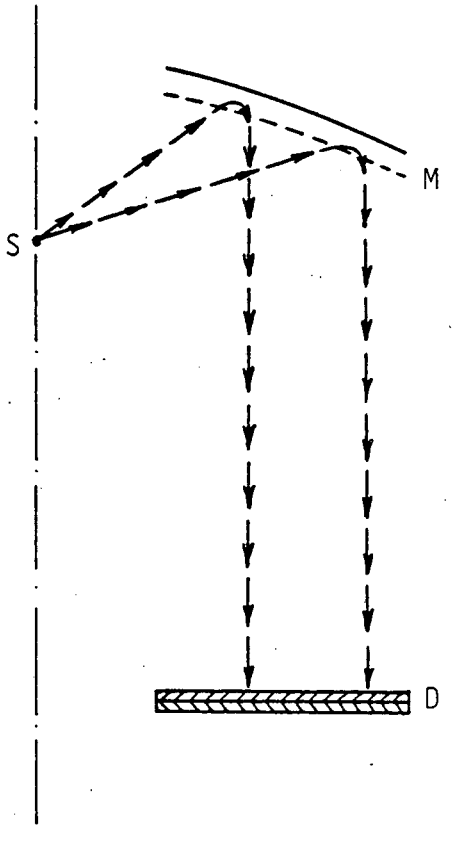

Figure 1

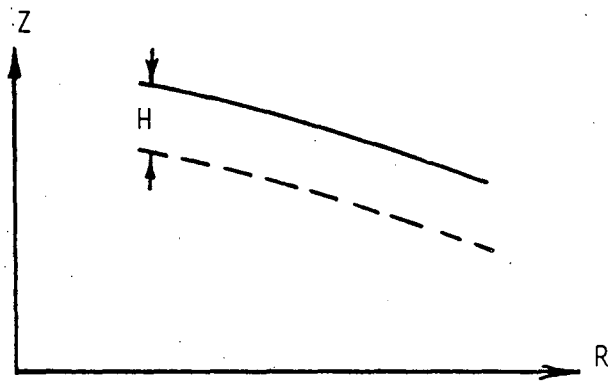

Figure 2

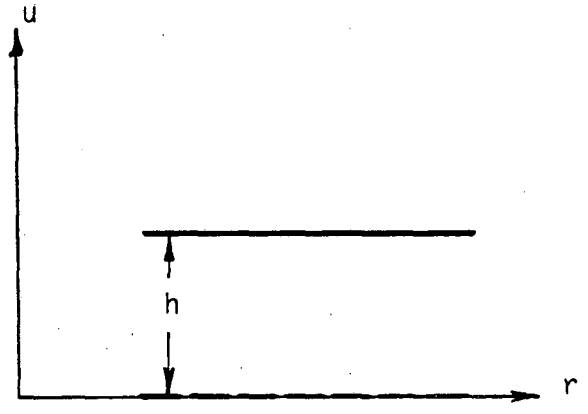

Figure 3

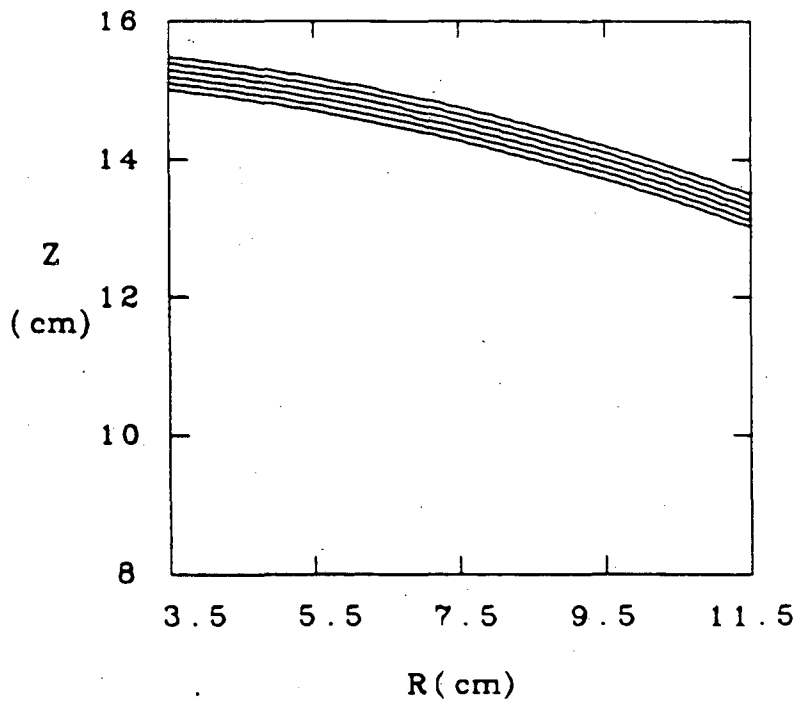

Figure 4

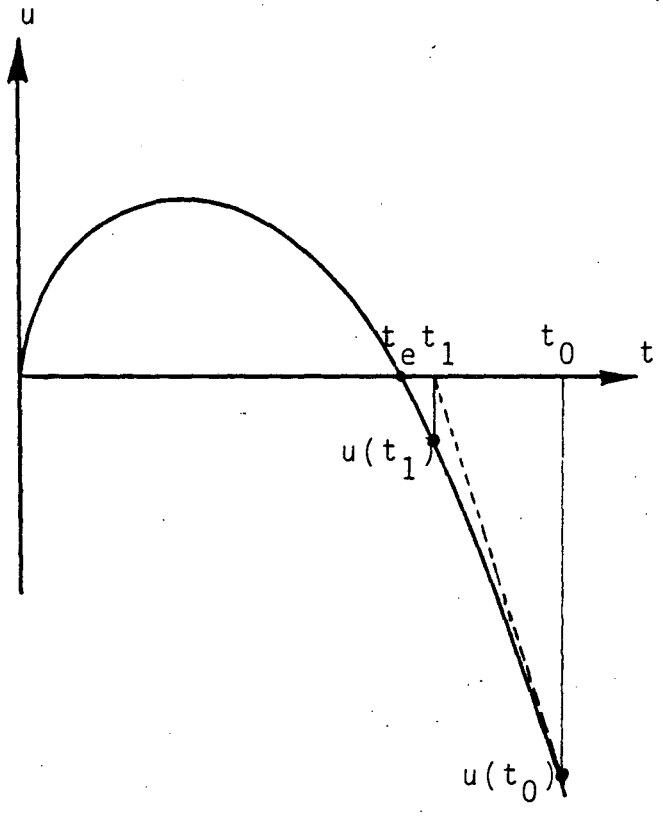

Figure 5

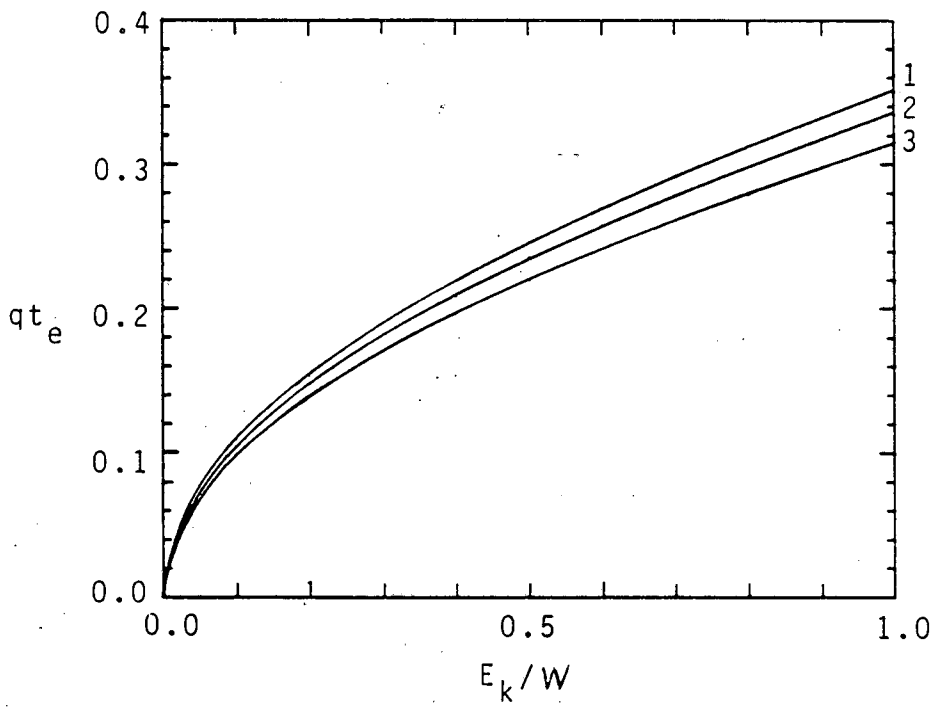

Figure 6

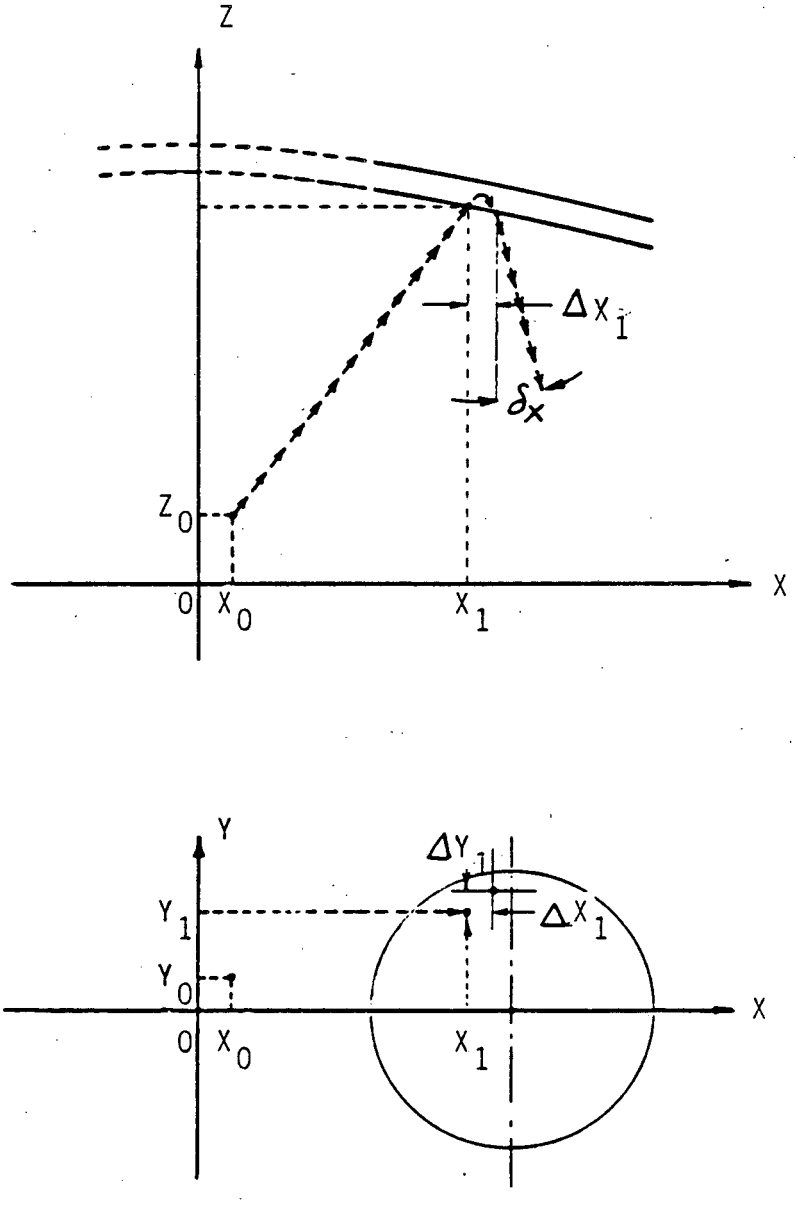

Figure 7

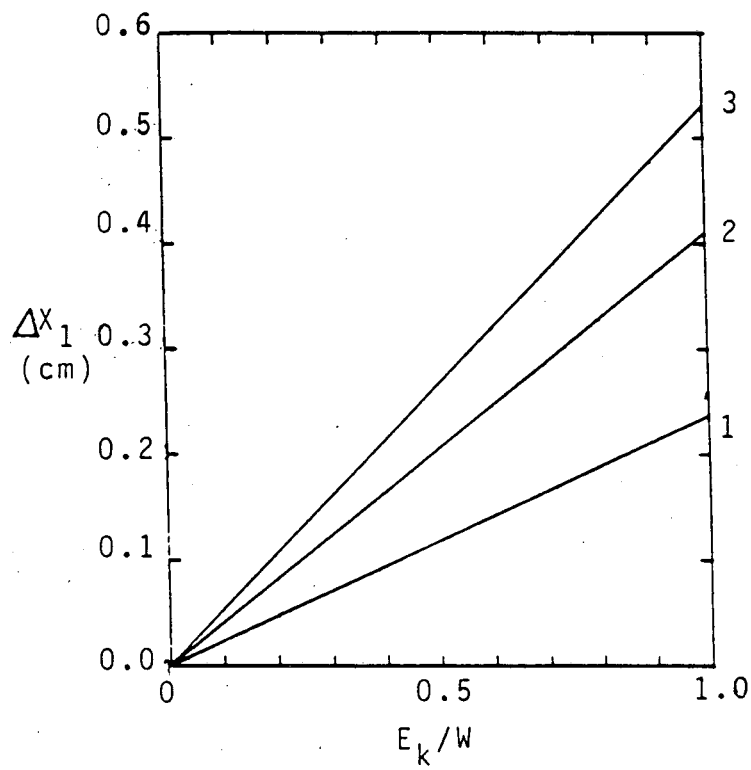

Figure 8

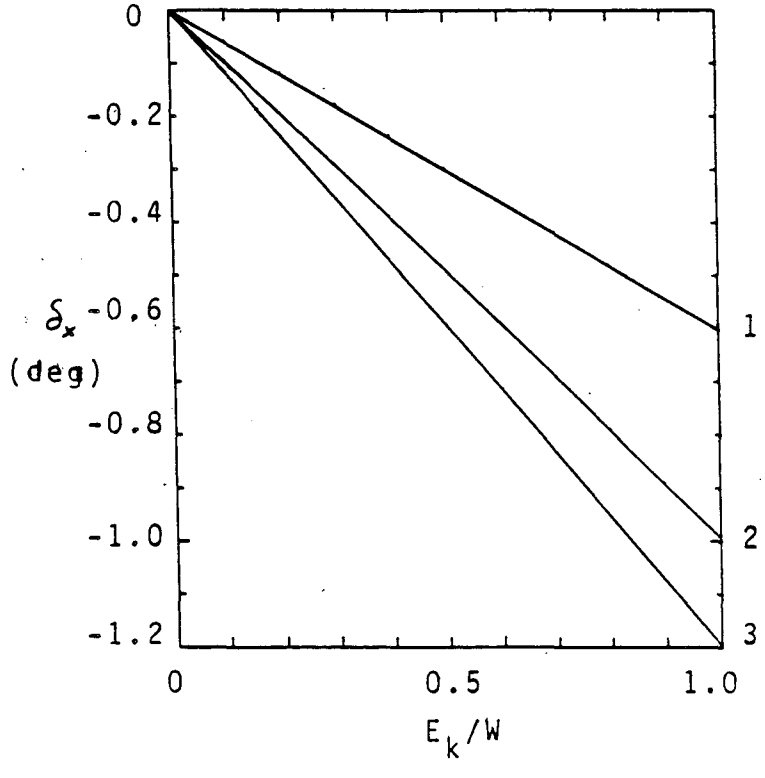

Figure 9

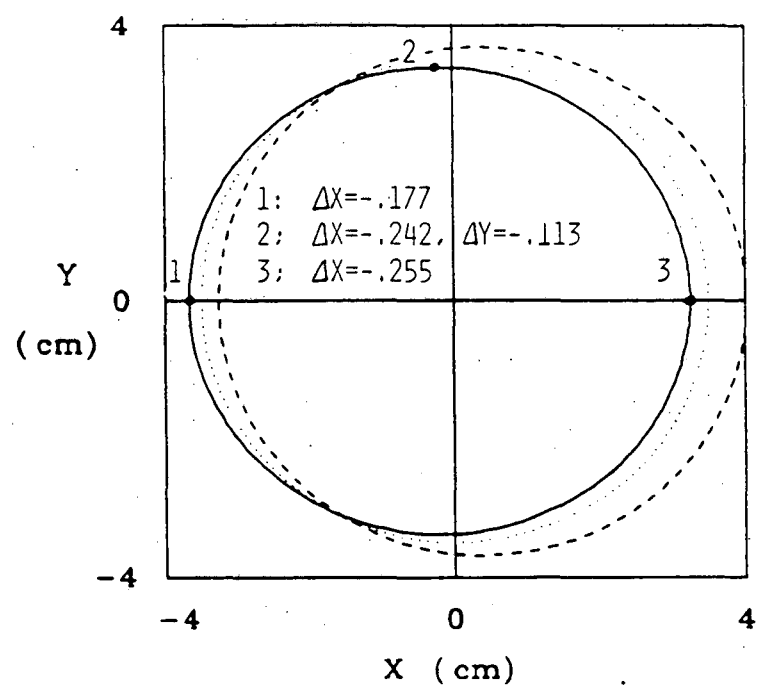

Figure 10

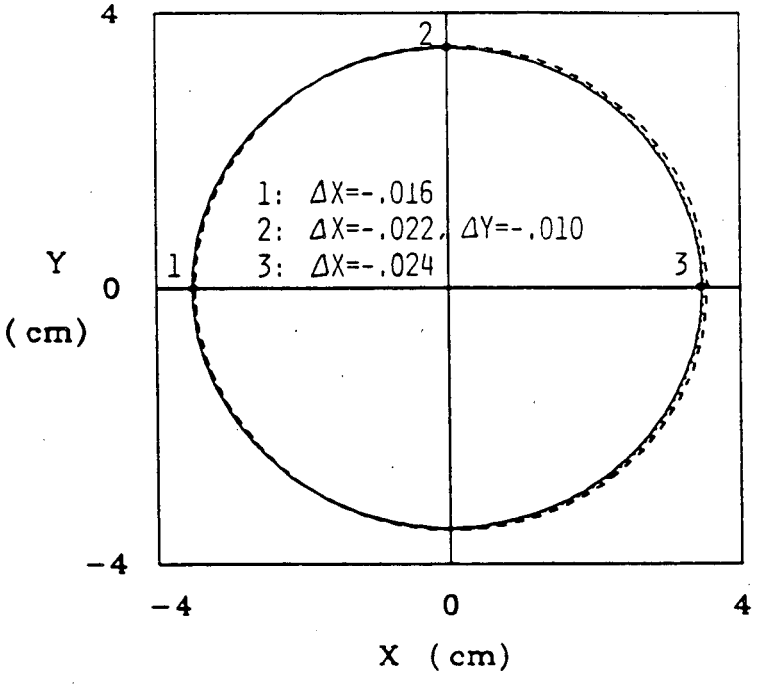

Figure 11

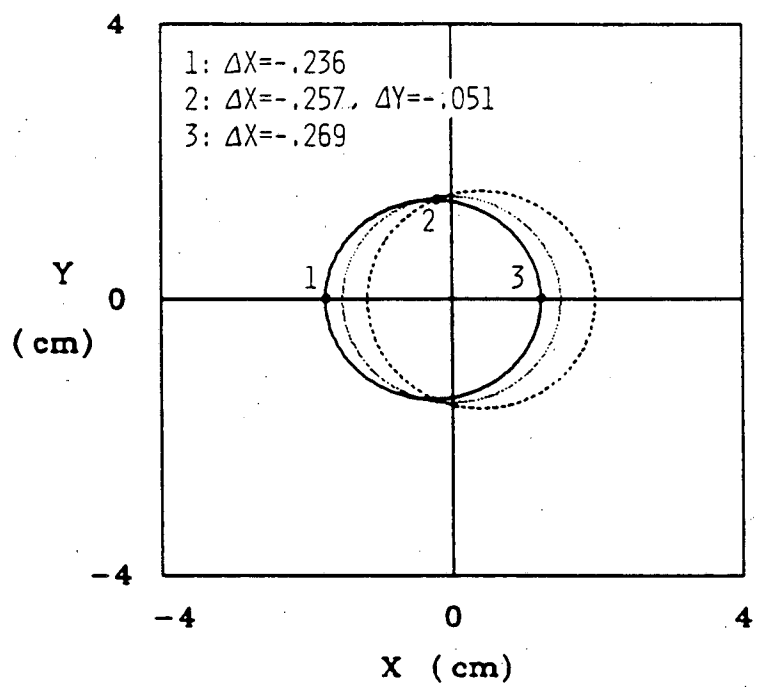

Figure 12

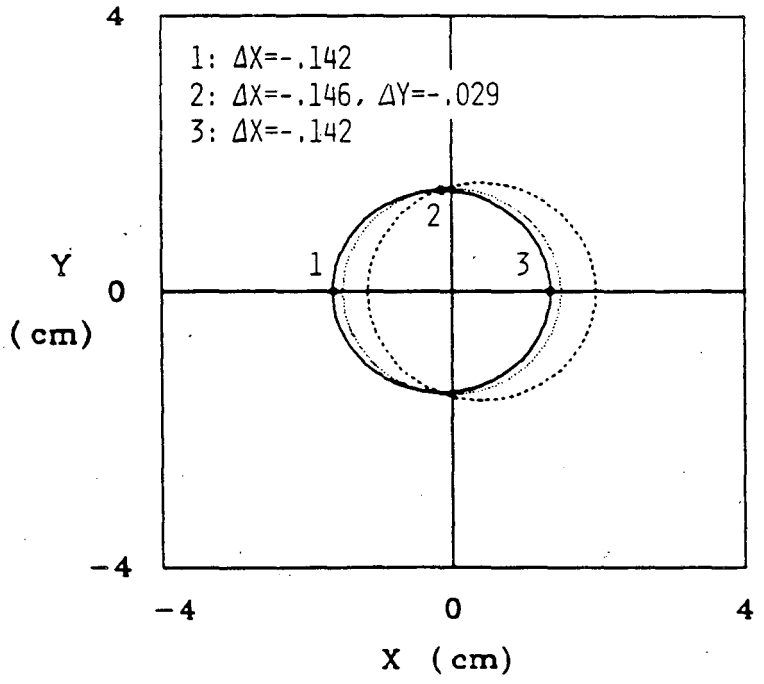

Figure 13

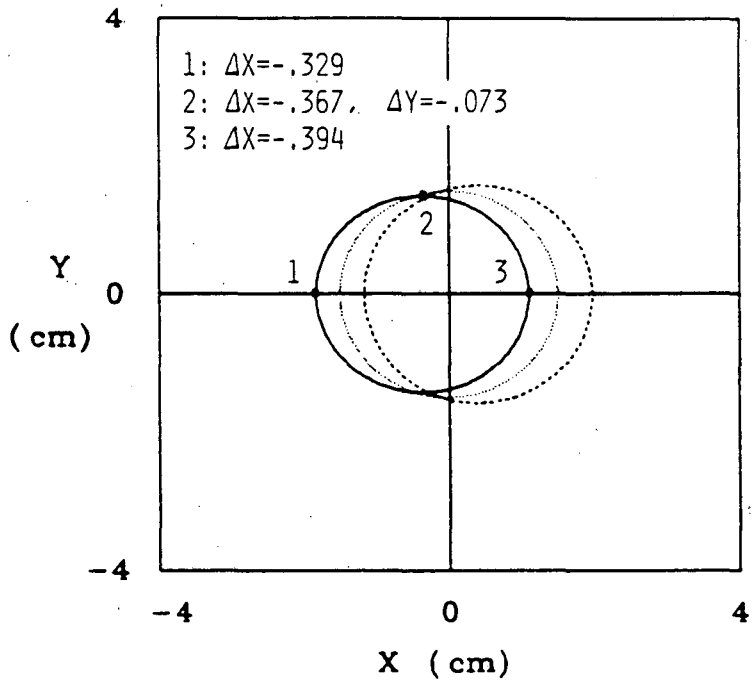

Figure 14

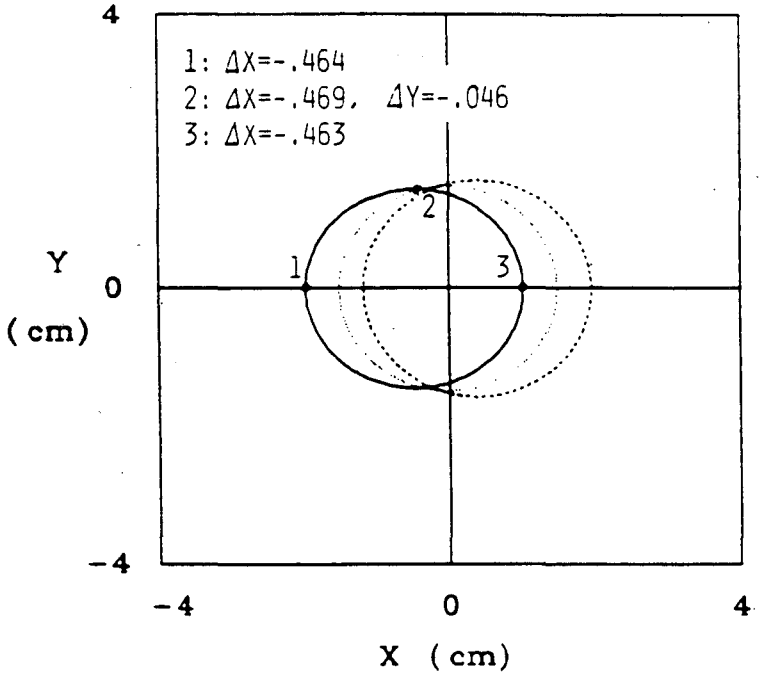

Figure 15

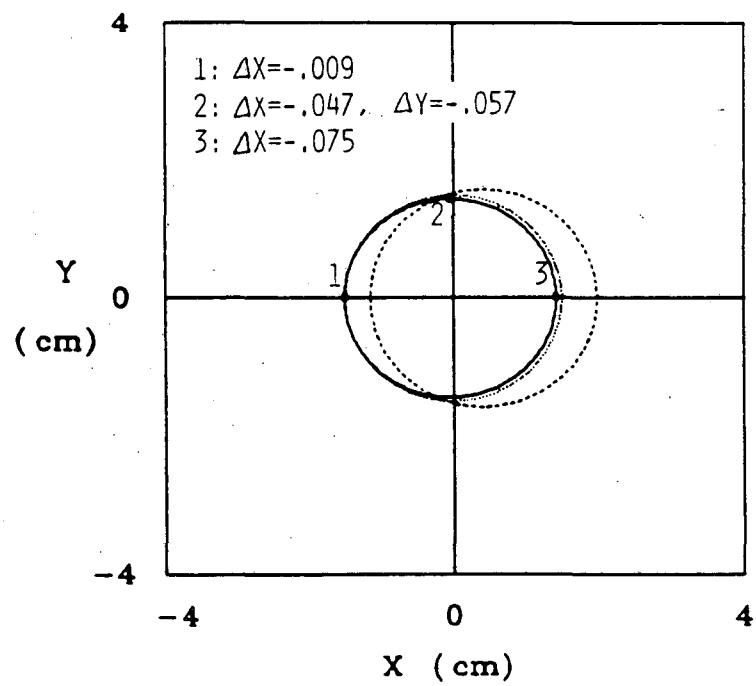

Figure 16

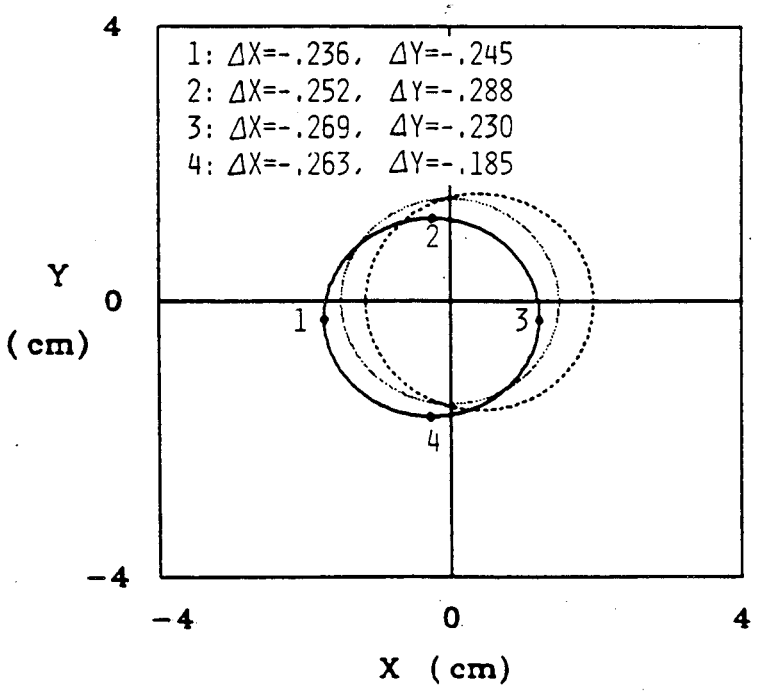
1: ΔX=-.236, ΔY=-.245
2: ΔX=-.252, ΔY=-.288
3: ΔX=-.269, ΔY=-.230
4: ΔX=-.263, ΔY=-.185
4
0
-4
Y
(cm)
-4
0
4
X (cm)
1
2
3
4

Figure 17

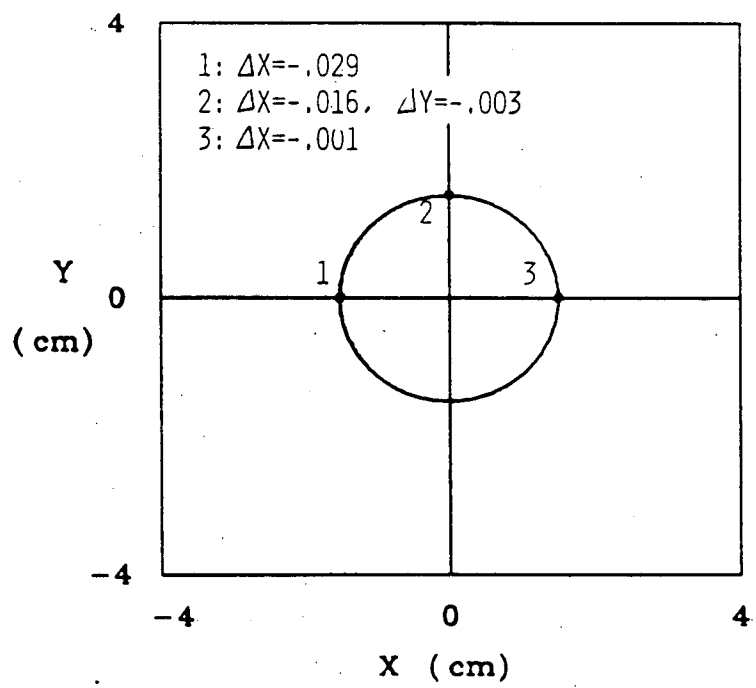

Figure 18

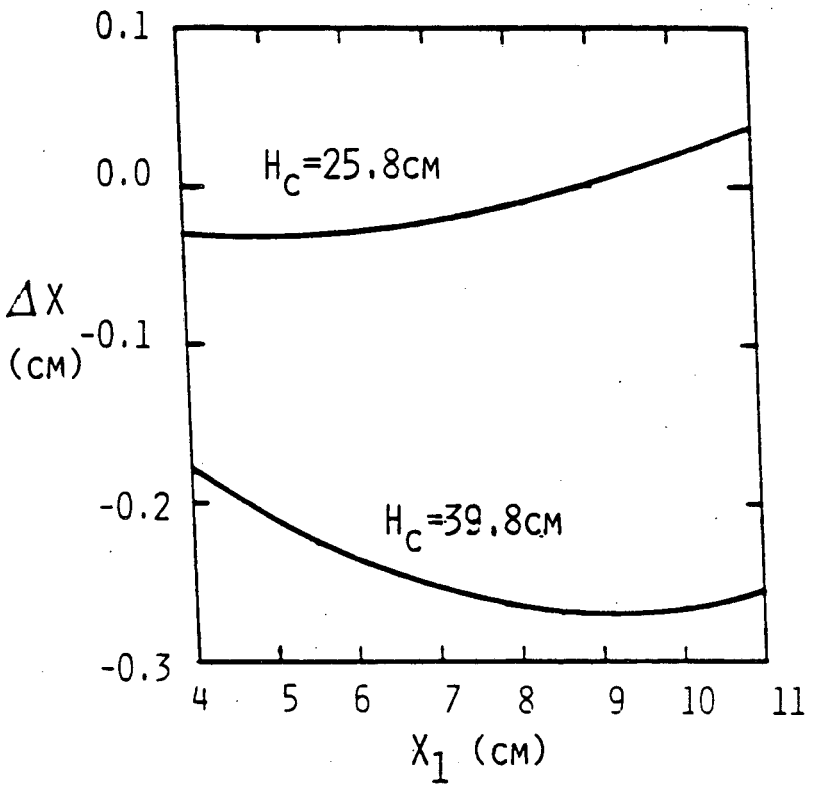

Figure 19

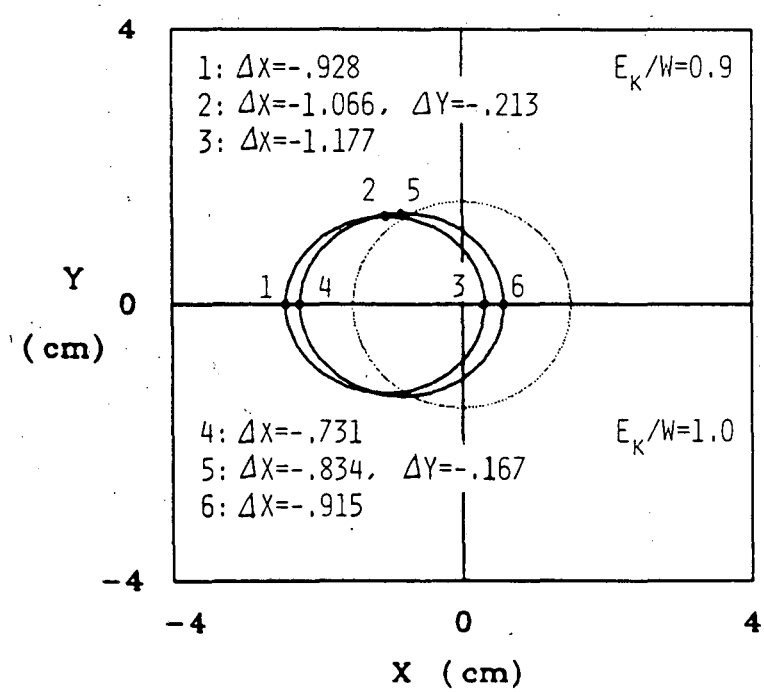
4
0
-4
Y
(cm)
-4
0
4
X (cm)
1: ΔX=-.928
2: ΔX=-1.066, ΔY=-.213
3: ΔX=-1.177
E_K/W=0.9
4: ΔX=-.731
5: ΔX=-.834, ΔY=-.167
6: ΔX=-.915
E_K/W=1.0
1
2
3
4
5
6

Figure 20

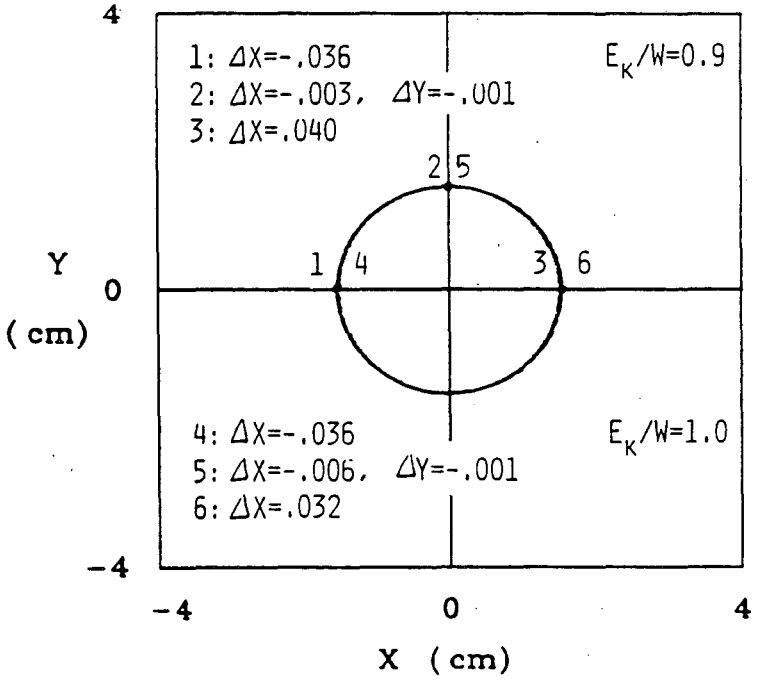
4
1: ΔX=-.036
2: ΔX=-.003, ΔY=-.001
3: ΔX=.040
E_K/W=0.9
2 5
Y
0
(cm)
1 4
3 6
4: ΔX=-.036
5: ΔX=-.006, ΔY=-.001
6: ΔX=.032
E_K/W=1.0
-4
-4
0
4
X (cm)

Figure 21

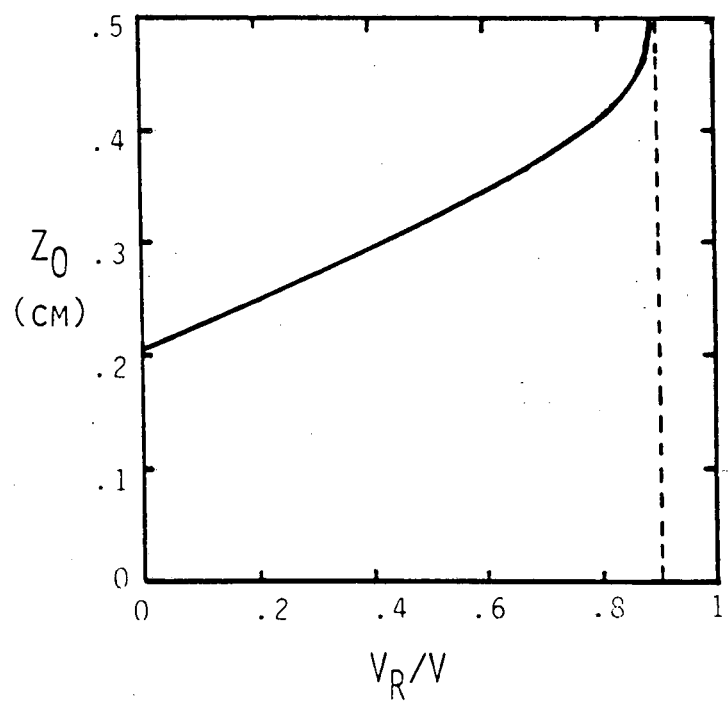

Figure 22

This report was done with support from the Department of Energy. Any conclusions or opinions expressed in this report represent solely those of the author(s) and not necessarily those of The Regents of the University of California, the Lawrence Berkeley Laboratory or the Department of Energy.

Reference to a company or product name does not imply approval or recommendation of the product by the University of California or the U.S. Department of Energy to the exclusion of others that may be suitable.

TECHNICAL INFORMATION DEPARTMENT
LAWRENCE BERKELEY LABORATORY
UNIVERSITY OF CALIFORNIA
BERKELEY, CALIFORNIA 94720